Numerical analysis and design of slender concrete-filled elliptical hollow section columns and beam-columns

W. Qiu[1], F. McCann[2]*, A. Espinos[3], M. L. Romero[3], L. Gardner[1]

Abstract

A numerical model simulating the behaviour of elliptical concrete-filled columns under either concentric or eccentric compressive load has been developed in ABAQUS. The numerical results have been compared against a range of experimental results for ultimate load, load–deflection behaviour and failure modes, with good agreement observed. An extensive parametric study has been undertaken whereby the slenderness, load eccentricity, cross-sectional geometry and reinforcement ratio of the concrete-filled columns were varied, creating a data set upon which to formulate design guidance since currently there are no specific provisions in the European Standard EN 1994-1-1 [1] for the design of concrete-filled steel elliptical section columns or beam-columns. It is shown that the current provisions of EN 1994-1-1 [1] for the design of concrete-filled steel columns of circular or rectangular cross-section are also appropriate for the design of members of elliptical cross-section, employing either buckling curve b or c, depending on the level of steel reinforcement. Finally, an assessment is made of the reliability of the design proposals for concrete-filled elliptical hollow section columns and beam-columns.

Numerical analysis and design of slender concrete-filled elliptical hollow section columns and beam-columns

W. Qiu[1], F. McCann[2]*, A. Espinos[3], M. L. Romero[3], L. Gardner[1]

[1] Department of Civil and Environmental Engineering, South Kensington Campus, Imperial College London, SW7 2AZ, UK.

[2] Department of Urban Engineering, School of the Built Environment and Architecture, London South Bank University, London SE1 0AA, UK

[3] Instituto de Cienca y Tecnología del Hormigón (ICITECH), Universitat Politècnica de València, València, Spain

*Corresponding author. Telephone: +44 20 7815 7152. Email: mccannf@lsbu.ac.uk

Abstract

A numerical model simulating the behaviour of elliptical concrete-filled columns under either concentric or eccentric compressive load has been developed in ABAQUS. The numerical results have been compared against a range of experimental results for ultimate load, load–deflection behaviour and failure modes, with good agreement observed. An extensive parametric study has been undertaken whereby the slenderness, load eccentricity, cross-sectional geometry and reinforcement ratio of the concrete-filled columns were varied, creating a data set upon which to formulate design guidance since currently there are no specific provisions in the European Standard EN 1994-1-1 [1] for the design of concrete-filled steel elliptical section columns or beam-columns. It is

shown that the current provisions of EN 1994-1-1 [1] for the design of concrete-filled steel columns of circular or rectangular cross-section are also appropriate for the design of members of elliptical cross-section, employing either buckling curve b or c, depending on the level of steel reinforcement. Finally, an assessment is made of the reliability of the design proposals for concrete-filled elliptical hollow section columns and beam-columns.

Keywords: composite structures; concrete-filled steel tubes; design of structures; elliptical sections; EN 1994-1-1; tubular sections

Symbols

Latin script symbols

a	major axis outer radius
A_a	cross-sectional area of steel tube
A_c	cross-sectional area of concrete
A_s	cross-sectional area of steel reinforcement
b	minor axis outer radius
e_f	flow potential eccentricity for concrete damage plasticity model
e_y	load eccentricity in the y direction
e_z	load eccentricity in the z direction

E_a	modulus of elasticity of steel tube
E_{cm}	secant modulus of elasticity of concrete
E_s	modulus of elasticity of steel reinforcement
$(EI)_{eff}$	effective flexural stiffness
$(EI)_{eff,II}$	effective flexural stiffness taking second-order effects into account
f_{b0}	compressive strength of concrete under biaxial loading
f_c	compressive strength of unconfined concrete
f_{cc}	compressive strength of confined concrete
f_s	yield strength of steel reinforcement
f_y	yield strength of steel tube
I_a	second moment of area of steel tube cross-section
I_c	second moment of area of concrete cross-section
I_s	second moment of area of steel reinforcement
k	design factor to account for second-order effects
K_c	second stress invariants on the tensile and compressive meridians
L	length of specimen
M_{Ed}	design moment
$M_{u,exp}$	second-order inelastic ultimate moment
N_{cr}	elastic critical buckling load
$N_{cr,eff}$	effective elastic critical buckling load for calculating second-order moments
N_{Ed}	design axial load
N_u	ultimate load
$N_{u,exp}$	experimental ultimate load
$N_{u,EC4}$	design ultimate capacity of columns according to EN 1994-1-1 [1]

$N_{u,FEA}$ ultimate load predicted by finite element analysis

$N_{pl,Rd}$ plastic resistance of cross-section in compression according to EN 1994-1-1 [1]

t steel tube wall thickness

Greek script symbols

ε_c strain at f_c

χ buckling reduction factor

Δ axial displacement

$\bar{\lambda}$ nondimensional global slenderness

μ viscosity parameter for concrete damage plasticity model

ρ reinforcement ratio

ψ dilation angle for concrete damage plasticity material model

ω_g initial global imperfection amplitude

ω_u mid-height lateral deflection at ultimate load

1. Introduction

In recent years, concrete-filled steel tubular (CFST) columns have gained increasing usage and popularity owing to a number of benefits that they offer over plain concrete or hollow steel columns. These benefits include greater cross-sectional resistance for the same footprint, greater stability of slender cross-sections, enhanced fire resistance, no requirement for temporary formwork and greater resistance to seismic loads [2,3]. With

the advent of high strength concrete and more effective and reliable pouring and pumping techniques, there has been a significant increase in the application of CFST members globally in the past two decades, particularly in China [4]. Previous investigations into the structural performance of CFST elements have been varied, and have included studies into the material behaviour of the composite sections [5-7], the testing of stub columns [8-11], concrete-filled stainless steel columns [12-14] and the testing of slender columns [15-17]. A comprehensive review of practical applications of CFST columns is provided in [18].

Existing studies [5-17] into the structural behaviour of CFST sections have generally focussed on circular, square and rectangular hollow sections (CHS, SHS and RHS, respectively). In the past fifteen years, steel elliptical hollow sections (EHS) have gained increased practical interest due to their introduction and availability as hot-finished products [19], their aesthetic properties and their enhanced flexural properties compared to CHS tubes [20]. Studies investigating the behaviour of steel EHS members include testing under concentric and eccentric compression [21,22] and bending [23], the buckling of steel EHS columns [24] and beams [20,25], and the local buckling, postbuckling [26] and ultimate strength [27] of slender elliptical hollow sections. These studies provided a basis upon which design rules for steel EHS members have been formulated [28], including rules for compressive resistance [21], bending [23], flexural buckling [24] and shear [29]. In the context of concrete-filled elliptical hollow section (CFEHS) members, previous experimental studies include compression testing of stub columns [4,30,31], members in bending [32], concentrically-loaded slender columns [33] and eccentrically-loaded columns [34–37]. The behaviour of CFEHS columns in fire conditions was also examined by [35].

Numerical studies of the behaviour of concrete-filled structural members include the modelling of the material behaviour of confined concrete [5-7], simulations of the behaviour of CFST stub columns [10] and complementary analytical modelling of the behaviour of CFST members [38]. Numerical analysis of concrete-filled CHS, SHS and RHS stub columns has been conducted by [39]. Previous numerical studies of CFEHS tubes have included the examination of short columns in axial compression [40], slender columns under axial compression [41] and columns in fire conditions under axial and eccentric compression [42].

In Section 2 of this paper, a summary of previous experiments on CFEHS columns is presented, along with key results from those experiments. The development of a finite element model of CFEHS members under either concentric or eccentric compressive load is then described, followed by a presentation of the validation of the numerical model against the experimental results. The details and results of an extensive parametric study are described, followed by comparisons with existing guidance from the European Standard EN 1994-1-1 [1] for the design of concrete-filled columns of circular or rectangular section. Finally, a reliability assessment, based on the results of the previous experiments, the parametric study and the predictions of the current design method of EN 1994-1-1 [1], is presented.

2. Review of experimental studies on CFEHS members

In this section, a summary of previous experimental studies of CFEHS columns is provided, along with the test results and a brief description of the test methodologies. While testing was conducted by [4,30,31] on CFEHS stub columns, the present study focuses on more slender columns. The three main experimental studies used for validation of the numerical model and the assessment of design proposals in the present study are [34–36]. The geometric and material properties, reinforcement ratios ρ, nondimensional slenderness $\bar{\lambda}$ (defined in Section 4.1) and ultimate loads recorded by [34–36] are summarised in Table 1. The cross-sectional geometry of the tested specimens is shown in Figure 1. A total of 48 tests from [34–36] were used for validation of the numerical model presented in Section 3.

In the experimental study described in [34], a total of 24 concrete-filled slender columns of 150 × 75 × 6.3 EHS cross-section and various lengths, either with or without steel reinforcement and loaded in compression either concentrically or eccentrically, were tested. The ends of the columns were fitted with knife-edges, resulting in the boundary conditions in the intended axis of bending and buckling being pinned-pinned while in the orthogonal direction, no end rotations were permitted.

An investigation into the fire resistance of CFEHS columns of 220 × 110 × 12 EHS cross-section carried out by [35] also included 6 tests at room temperature, 3 of which also possessed steel reinforcement. The specimens were loaded either concentrically or eccentrically, with knife-edges attached to the ends of the columns, which were orientated such that buckling occurred about the minor axis in all tests. When testing specimen RE-00, a 2 mm load eccentricity was included to encourage buckling to initiate in a single particular direction.

The investigation of [36] into the behaviour of CFEHS beams and columns included 6 tests on concentrically-loaded concrete-filled columns and 8 tests on eccentrically-loaded concrete-filled columns of 192 × 124 × 3.82 EHS cross-section. None of the specimens contained steel reinforcement. The specimens were orientated with respect to knife-edge fittings at the ends of the columns so that buckling about the major axis was enforced in all tests.

3. Numerical analysis

In this section, a numerical model developed to simulate the behaviour of CFEHS columns and beam-columns is described. The model was validated against the experimental results of [34–36] by comparing ultimate loads, load–deflection behaviour and failure modes. Once satisfactory agreement between the experimental and numerical results was achieved, an extensive parametric study comprising 360 simulations was conducted, in which the cross-sectional geometry, reinforcement ratio, reinforcement cover, column slenderness and load eccentricity were varied.

3.1 Description of finite element model

The numerical model was developed using the ABAQUS [43] finite element (FE) software. In the following subsections, the mesh, material models, boundary conditions and analysis approach used in the simulations are described.

3.1.1 Geometry and mesh

In keeping with [41,42], solid 8-noded reduced integration C3D8R elements were used to model both the concrete core and the steel tube, while B31 beam elements were used to model the reinforcing bars. The characteristic element size was 10 mm. Rigid R3D4 shell elements were used to model the end-plates, through which the load was applied to the members.

3.1.2 Material modelling

The stress–strain behaviour of both the steel tube material and the steel reinforcement material was represented using a multi-linear elastic–plastic model with isotropic hardening, based on tensile tests conducted on steel coupons cut from the EHS test specimens and the rebar. The multi-linear stress-strain curves comprised 50 intervals to ensure that the full range of the response could be captured accurately, a typical example of which is shown in Figure 2. The measured steel material properties given in Table 1 were employed during the validation of the model, while characteristic values were used in the parametric study.

In order to account for the effect of confinement by the tube walls and reinforcement, a confined concrete stress–strain model based on that proposed by [40] was adopted; this model was also used by [41]. It was found by [40] that use of the stress–strain curve model proposed by [44], which was originally calibrated against tests on circular section columns, was not appropriate for use with elliptical sections since the confinement effect varies along the circumference of the section . An alternative stress–strain model, which considered the average confinement effect along the circumference of the elliptical section, was proposed by [40] for use with CFEHS members and has been

adopted in the present study; a typical comparison between the stress-strain curves of concrete (with f_c = 30 N/mm^2) in the unconfined and confined (by a 150×75×6.3 steel EHS) conditions is presented in Figure 3.

The confined stress–strain curves were used in the present study in conjunction with the concrete damaged plasticity model employed in ABAQUS [43] using the following parameters: the ratio of the second stress invariants on the tensile and compressive meridians K_c was taken equal to 0.667, the dilation angle ψ equal to 15º, the flow potential eccentricity e_f was taken equal to 0.1, the viscosity parameter μ was taken as zero and the ratio of the compressive strength of concrete under biaxial loading f_{b0} to the uniaxial compressive strength of concrete f_c was taken equal to 1.16, following the recommendations of [39].

Following guidance from ACI 318 [45], the modulus of elasticity E_c of the initial linear elastic portion of the concrete stress–strain curve was defined as:

$$E_c = 4700\sqrt{f_c} \quad (1)$$

where E_c and f_c are in MPa. The Poisson's ratio of concrete was set at 0.2 [39]. The uniaxial tensile response was assumed to be linear until the tensile strength of the concrete was reached, which was taken as $0.1f_c$ [46]. Thereafter, the inelastic portion of the tensile stress–strain curve was modelled as 10% of the compressive stress-strain curve [41].

3.1.3 Boundary conditions and interactions

Owing to the symmetrical boundary conditions of the test setup and doubly-symmetric cross-sectional geometry of the CFEHS members, a model representing half the cross-

section and half the buckling length of the columns was modelled in ABAQUS [43], as shown in Figure 4, with symmetry boundary conditions defined on the appropriate surfaces. At the ends of the columns, rotation about the intended buckling axis was permitted but rotation about the other cross-sectional axis was prevented, thus replicating the knife-edge boundary conditions employed in the experiments. The compressive load was applied by means of displacement control to a reference point located on the rigid end-plate at an appropriate distance from the geometric centroid of the elliptical section to model the load eccentricity. Tie constraints were defined between the steel tube and the rigid end-plate. The interactions between the concrete core and the steel tube, and the concrete core and the end-plates were modelled with hard contact behaviour in the normal direction. For the tangential contact behaviour, it was found by [40] that varying the coefficient of friction between 0.1 and 0.5 had no significant influence on the overall behaviour of the model. A value of 0.3 was applied in the present study.

3.1.4 Analysis procedure

In order to provide an initial imperfection mode shape, a linear eigenvalue analysis was conducted for each column model. The global buckling (as opposed to local buckling) mode with the lowest eigenvalue was selected as the initial imperfect geometry. For the validation of the models, the measured imperfection amplitudes from the corresponding experiments were used. In some instances in [34], the geometrical imperfections were too small to measure directly, so values determined from a Southwell plot were employed. Also, in keeping with the test procedure, a load eccentricity of (L/1000 + 2 mm) was included when modelling specimen RE-00 [35]. For the parametric study, an imperfection amplitude of L/1000 was used throughout. After incorporation of the

imperfection, a geometrically-nonlinear displacement-controlled static analysis was performed.

3.2 Validation of FE model

In order to assess the accuracy of the numerical model, comparisons were made between the ultimate loads and load–displacement curves obtained from a series of experiments [34-36] and those predicted by the numerical model. A group of the experimental results [33] were not used for the model validation owing to some unexpected trends in some of the reported data. Measured values of material strength and member geometry including imperfections were applied in the models. The reinforced specimens tested by [34,35] contained four reinforcing bars of 10 mm diameter.

Good agreement between the ultimate loads obtained from the numerical model $N_{u,FEA}$ and the experimental ultimate loads $N_{u,exp}$ can be observed in Figure 5 and Table 2. The ability of the numerical models to capture the load–deflection behaviour accurately is demonstrated by the good agreement between the experimental and numerical curves presented in Figures 6 to 8 for specimens [34] buckling about the major axis, specimens buckling about the minor axis and specimens containing steel reinforcement, respectively. From the example of specimen E6:L1-MA-50 [34], it can be seen from Figure 9 that good agreement was also achieved between the experimental and numerical failure modes; the corresponding load-deflection behaviour for this specimen is shown in Figure 6.

3.3 Parametric study

After achieving satisfactory agreement between the results of the experiments and the numerical analysis, a parametric study using the validated FE models was conducted. The parameters varied in the study were the cross-sectional geometry $2a \times 2b \times t$, the nondimensional slenderness $\bar{\lambda}$, the steel reinforcement ratio ρ, the minor axis reinforcement cover u_s, the intended buckling axis and the load eccentricities e_y and e_z, which are shown in Figure 10. Specimens modelled with steel reinforcement contained six reinforcing bars, with the bar diameter chosen to provide the specified reinforcement ratio. The ranges of values assumed by these parameters are given in Table 3. Characteristic material strengths f_y, f_c and f_s of the steel tube, concrete and steel reinforcement, respectively, were adopted in the parametric study and are also given in Table 3, while the amplitude of the imperfection included in the model was $L/1000$. The shape of the steel stress-strain curve used in the parametric study was taken as that from the validation study, but characteristic material strengths were used in place of the measured values, as illustrated in Figure 2. The 220 × 110 × 12.5 specimens were not modelled with steel reinforcement since the EN 1992-1-1 [47] requirements regarding minimum bar spacing cannot be met. The results from the parametric study are examined in Section 4. The combined experimental and numerical data set is then used to devise design recommendations for CFEHS columns and beam-columns.

4. Analysis of results and design recommendations

In this section, the results of the parametric study are analysed, and the ultimate loads from the tests and numerical models are compared with the resistances determined according to the provisions of EN 1994-1-1 [1] for members under axial compression

and for members under combined compression and uniaxial bending. Since there are no specific provisions for elliptical hollow section members, comparisons were made using the provisions for circular and rectangular sections. It was found previously [34–36] that the code predictions generally agreed well with the experimental results.

4.1 Members in axial compression

For columns in axial compression, it is stated in EN 1994-1-1 [1] that the nondimensional slenderness $\bar{\lambda}$ of a composite member may be used to calculate the buckling reduction factor χ using the buckling curves provided in EN 1993-1-1 [48]. The resulting reduction factor is multiplied by the plastic resistance of the cross-section to compression $N_{\mathrm{pl,Rd}}$ to provide the axial design resistance $N_{\mathrm{u,EC4}}$ of the concentrically-loaded column. The nondimensional slenderness $\bar{\lambda}$ is defined as:

$$\bar{\lambda} = \sqrt{\frac{N_{\mathrm{pl,Rd}}}{N_{\mathrm{cr}}}}. \tag{2}$$

The plastic resistance to compression $N_{\mathrm{pl,Rd}}$ of a concrete-filled hollow section is given in EN 1994-1-1 [1] as:

$$N_{\mathrm{pl,Rd}} = A_{\mathrm{a}} f_{\mathrm{y}} + A_{\mathrm{c}} f_{\mathrm{c}} + A_{\mathrm{s}} f_{\mathrm{s}} \tag{3}$$

where A_{a}, A_{c} and A_{s} are the cross-sectional areas of the steel tube, concrete core and steel reinforcement, respectively, and f_{y}, f_{c} and f_{s} are the strengths of the steel tube, concrete and steel reinforcement, respectively. For CHS columns with $\bar{\lambda} < 0.5$ and $e/D < 0.1$ (where D is the diameter of the CHS), the contribution of the concrete is amplified to take into account the increased confinement effect. As was shown by testing [4] and numerical modelling [40], the confinement effect in an EHS is somewhat less than that in a CHS, and so in the present study, the coefficient of the contribution of the concrete to the plastic resistance to compression is set to 1.0, as would be applied to a concrete-

filled member with a square or rectangular cross-section. The elastic critical buckling load N_{cr} for a composite member is:

$$N_{cr} = \frac{\pi^2 (EI)_{eff}}{L^2} \tag{4}$$

where the effective flexural stiffness of the composite cross-section $(EI)_{eff}$ is given in EN 1994-1-1 [1] by:

$$(EI)_{eff} = E_a I_a + 0.6\, E_c I_c + E_s I_s \tag{5}$$

and E_a, E_c and E_s are the moduli of elasticity of the steel tube, concrete and steel reinforcement, respectively, and I_a, I_c and I_s are the second moments of area of the steel section, concrete section and the reinforcement about the buckling axis in question.

According to the current provisions of EN 1994-1-1 [1] for concrete-filled CHS and RHS members, the buckling curve that should be used is dependent upon the reinforcement ratio ρ. For $\rho \leq 3\%$, curve a is prescribed, while for $3\% < \rho \leq 6\%$ curve b should be used. In Figure 11, the ultimate resistances N_u from the previous tests and those from the numerical parametric study are normalized by the plastic resistance of the cross-section $N_{pl,Rd}$, and plotted against slenderness $\bar{\lambda}$. The results have been grouped by reinforcement ratio - $\rho \leq 3\%$ and $3\% < \rho \leq 6\%$. The results are compared to EN 1993-1-1 [48] buckling curves a, b and c, where it can be seen that curves b tends to provide a lower bound for specimens with a low level of reinforcement, while curve c tends to provide a lower bound to specimens with a higher level of reinforcement. It is thus proposed that when designing CFEHS columns with $\rho \leq 3\%$, curve b should be used, while for $3\% < \rho \leq 6\%$, curve c should be used.

In Figure 12, the experimental and numerical results for concentrically-loaded CFEHS members are compared to the design resistances calculated using curves b and c. In Figure 13 variation of the ratios of the experimental and numerical results to the design resistances calculated using curves b and c with slenderness are plotted, where it can be seen that the use of the revised buckling curves tends to provide safe predictions of the design resistance.

4.2 Members in combined compression and uniaxial bending

For eccentrically-loaded columns, the effects of combined compression and bending must be accounted for. The first-order design moment M_{Ed} arising from the effects of the eccentric application (with eccentricity e) of the axial load N_{Ed} and the initial imperfection ω_{g} is:

$$M_{\mathrm{Ed}} = N_{\mathrm{Ed}} \, (e + \omega_{\mathrm{g}}). \tag{6}$$

The magnitude of the initial imperfection ω_{g} is given by EN 1994-1-1 [1] for CHS and RHS members as $L/300$ for members with a reinforcement ratio $\rho \leq 3\%$ and $L/200$ for $3\% < \rho \leq 6\%$. Second-order effects arising from the lateral deflection of the column are accounted for by amplifying M_{Ed} by a factor k, defined as:

$$k = \frac{\beta}{1 - N_{\mathrm{Ed}} / N_{\mathrm{cr,eff}}}. \tag{7}$$

where β is an equivalent moment factor set to 1.1 for equal and opposite end moment loading and the elastic critical buckling load $N_{\mathrm{cr,eff}}$ is calculated similarly to Eq.(4) except using the effective flexural stiffness $(EI)_{\mathrm{eff,II}}$ where:

$$(EI)_{\mathrm{eff,II}} = 0.9 \, (E_{\mathrm{a}} I_{\mathrm{a}} + 0.5 \, E_{\mathrm{c}} I_{\mathrm{c}} + E_{\mathrm{s}} I_{\mathrm{s}}). \tag{8}$$

Thus, the curve relating the axial load N_{Ed} to the second-order moment M_{Ed} is defined. The resistance of the composite column is then defined using cross-section moment–

axial load interaction curves. In the present study, the curves were derived using numerical integration to determine the level of bending moment $M_{\mathrm{pl},N,\mathrm{Rd}}$ that could be sustained for a given axial load, assuming fully plastic distributions of stresses and that the concrete did not act in tension. According to EN 1994-1-1 [1], for grades S275 and S355 steel, the following inequality must be satisfied:

$$\frac{M_{\mathrm{Ed}}}{M_{\mathrm{pl},N,\mathrm{Rd}}} \leq 0.9 \tag{9}$$

where $M_{\mathrm{pl},N,\mathrm{Rd}}$ is the plastic moment resistance of the composite column accounting for the presence of the axial load. For grades S420 and S460, the coefficient 0.9 is replaced by 0.8. The predicted design resistance $N_{\mathrm{u,EC4}}$ for the eccentrically-loaded column is given by the intersection of the loading and resistance curves, i.e., by determining the value of N_{Ed} for which $M_{\mathrm{Ed}} = 0.9\ M_{\mathrm{pl,N,Rd}}$.

In Figure 14, the experimental and numerical results are compared to the resistances calculated according to EN 1994-1-1 [1], while in Figure 15 the ratios of the experimental and numerical results to resistances determined according to EN 1994-1-1 [1] are plotted against slenderness. The trends of the results are discussed in Section 4.3 and a reliability analysis is presented in Section 5.

4.3 Influence of parameters on accuracy of design methods

In Figure 16, it can be seen that for different levels of load eccentricity, increasing the slenderness leads to different effects on the accuracy of the design methods. For concentrically-loaded specimens, the design method tends to become generally slightly more conservative with increasing slenderness. For a low level of load eccentricity, the accuracy of the design method remains somewhat constant and on the safe side, while for a high level of load eccentricity, the design method is most conservative for lower

slendernesses. As the slenderness increases, the design method becomes less conservative, though generally remains on the safe side. In Figure 17, it can be seen that the accuracy of the design methods is not as influenced by the level of reinforcement as by the level of load eccentricity, with a reasonable amount of scatter consistently present across the range of slendernesses. The observed discrepancies between the numerically derived and predicted resistances are attributed primarily to the simplifying assumptions (neglect of concrete in tension and interface conditions) made in the estimation of the flexural rigidity of the composite members in the design approach.

5. Reliability analysis

In this section, the reliability of the proposed design approaches for CFEHS under axial compression and combined axial compression and uniaxial bending are assessed through statistical analyses, according to the provisions of EN 1990 [49, 50]. A summary of the key calculated statistical parameters for the proposals is reported in Table 4, where $k_{d,n}$ is the design (ultimate limit state) fractile factor, b is the average ratio of test (or FE) to design model resistance based on a least squares fit to all data, V_δ is the COV of the tests and FE simulations relative to the resistance model, V_r is the combined COV incorporating both model and basic variable uncertainties, and γ_{M1} is the partial safety factor for member resistance. In the analyses, the COVs of the strength of steel, reinforcement bar and concrete were taken as 0.005 [51], 0.07 [52] and 0.18 [53] respectively, while the COVs of the geometric properties was taken as 0.03 [51], 0.06 [52] and 0.01 [53] respectively. The over-strength ratios for material yield strength were taken as 1.16 [51] and 1.34 [52] for steel and reinforcements, respectively, while the ratio for concrete was calculated from:

$$f_c = f_m - 1.64\,\delta \tag{10}$$

where f_c and f_m are the characteristic and mean values of compressive concrete strength and δ is the standard deviation [54]. As can be seen from Table 4 (a) and (b), the required partial factors for both the proposed design methods for CFEHS members under axial compression and combined compression and uniaxial bending are close to the currently adopted value of 1.0 in EN 1994-1-1 [1], and thus the proposed design methods are considered to satisfy the reliability requirements of EN 1990 [49].

6. Conclusions

A numerical model simulating the behaviour of CFEHS columns and beam-columns has been developed using the finite element analysis software ABAQUS [43]. The model was validated against the results of previous experimental programmes [34–36] by comparing predictions for ultimate load, load–axial displacement curves and failure modes. Once validated, an extensive parametric study comprising 360 specimens was conducted in which the cross-sectional geometry, column slenderness, steel reinforcement ratio, load eccentricity, intended axis of buckling and the cover to the reinforcement were varied.

The experimental and numerical results were compared with the provisions of EN 1994-1-1 [1] for slender concrete-filled CHS and RHS columns. It was found that, in general, the current provisions for the design resistances of members in axial compression were not satisfactory when compared with the experimental and numerical results. It is proposed for CFEHS members in axial compression that for $\rho \leq 3\%$, curve b should be used, while for $3\% < \rho \leq 6\%$ curve c should be used**.** It was found that when using the revised buckling curves, the resulting predicted design resistances tended to be safe

while not overly conservative. This was confirmed by means of reliability analysis to EN 1990 [49].

7. Acknowledgements

The authors would like to express their sincere gratitude to the European Union for the help provided through Project RFSR-CT-2012-00025, carried out with a financial grant from the Research Programme of the Research Fund for Coal and Steel.

Appendix: Design example

The compressive load-carrying capacity of a 400 × 200 × 12.5 concrete-filled EHS column 4 m in length is to be determined. The steel tube is of Grade S355 steel, while the concrete class is C30. It can be assumed that the member will buckle about its minor axis.

Step 1: Determine cross-sectional properties

$2a$ = 400 mm, $2b$ = 200 mm, t = 12.5 mm, L = 4 m

The area of concrete $A_c = \frac{\pi}{4}(2a-2t)(2b-2t) = \frac{\pi}{4}(400-2\times12.5)(200-2\times12.5) =$

$\Rightarrow A_c = \frac{\pi}{4}(400-2\times12.5)(200-2\times12.5) = 51542 \text{ mm}^2$

The area of steel $A_a = P_m t = \pi(a_m + b_m)\left(1+3\frac{h_m}{10+\sqrt{4-h_m}}\right)t$,

where P_m is the mean perimeter, $h_m = (a_m - b_m)^2/(a_m + b_m)^2$, $a_m = (2a - t)/2$ and $b_m = (2b - t)/2$ [21]

$\Rightarrow a_m = (400 - 12.5)/2 = 193.75$ mm, $b_m = (200 - 12.5)/2 = 93.75$ mm,

$h_m = (193.75 - 93.75)^2/(193.75 + 93.75)^2 = 0.121$

$$\Rightarrow A_a = \pi(193.75+93.75)\left(1+3\frac{0.121}{10+\sqrt{4-0.121}}\right)\times 12.5 = 11632 \text{ mm}^2$$

The second moment of area of concrete about the minor axis is:

$$I_{c,z} = \frac{\pi}{64}(2a-2t)(2b-2t)^3 = \frac{\pi}{4}(400-2\times12.5)(200-2\times12.5)^3 = 1.578\times10^9 \text{ mm}^4$$

The second moment of area of steel about the minor axis is:

$$I_{a,z} = \frac{\pi}{64}(2a)(2b)^3 - I_{c,z} = \frac{\pi}{4}(400)(200)^3 - 9.865\times10^7 \text{ mm}^4 = 9.348\times10^8 \text{ mm}^4$$

Step 2: Determine effective section properties

f_{yk} = 355 MPa, f_c = 30 MPa, E_a = 210000 MPa, E_c = 33000 MPa

$\Rightarrow f_{yd} = f_{yk}/\gamma_{M0}$ = 355 / 1.0 = 355 MPa, $f_{cd} = f_c/\gamma_C$ = 30 / 1.5 = 20 MPa

The plastic resistance to compression of the section is:

$N_{pl,Rd} = A_a f_{yd} + A_c f_{cd}$ = 11632 × 355 + 51542 × 20 = 5160 kN

The effective minor axis flexural rigidity is:

$(EI)_{eff,z} = I_a E_a + 0.6 I_c E_c = (9.348 \times 210000 + 0.6 \times 15.78 \times 33000) \times 10^8$

$= 2.276\times10^{14}$ N mm^2

The minor axis elastic critical buckling load is thus:

$N_{cr,z} = \pi^2(EI)_{eff,z} / L^2 = \pi^2(2.276 \times 10^{14}) / (4\times 10^3)^2 = 1.404\times 10^7$ N=14040kN

Step 3: Calculate buckling reduction factor

The nondimensional slenderness $\bar{\lambda} = \sqrt{\frac{N_{pl,Rd}}{N_{cr,z}}} = \sqrt{\frac{5160}{14040}} = 0.61$

Since there is no steel reinforcement, buckling curve b from EN 1993-1-1 (2005) shall be used, therefore α = 0.34.

$$\Rightarrow \Phi = 0.5\left(1+\alpha\left(\bar{\lambda}-\bar{\lambda}_0\right)+\bar{\lambda}^2\right) = 0.5\left(1+0.34\left(0.61-0.20\right)+0.61^2\right) = 0.756$$

$$\Rightarrow \chi = 1/\left(\Phi+\sqrt{\Phi^2-\bar{\lambda}^2}\right) = 1/\left(0.756+\sqrt{0.756^2-0.610^2}\right) = 0.832$$

$$\Rightarrow N_{b,Rd} = \chi N_{pl,Rd} = 0.832\times5160 = 4293 \text{ kN}$$

References

[1] Comité Européen de Normalisation. 2004. *EN 1994-1-1:2004 Eurocode 4: Design of composite steel and concrete structures – Part 1–1: General rules and rules for buildings*. British Standards Institute.

[2] Bergmann R., Matsui C., Meinsma C., Dutta, D. 1995. *Design Guide for Concrete Filled Hollow Section Columns under Static and Seismic Loading*, CIDECT Design Guide 5, CIDECT.

[3] Espinos A., Gardner L., Romero M.L., Hospitaler, A. 2011. Fire behaviour of concrete filled elliptical steel columns, *Thin-Walled Struct,*, **49**(2), 239–255.

[4] Yang H., Lam D., Gardner L. 2008. Testing and analysis of concrete-filled elliptical hollow sections, *Eng. Struct.*, **30**, 3771–3781.

[5] Mander J.B. Priestly M.J.N., Park R. 1988. Theoretical stress-strain model for confined concrete, *J. Struct. Eng., ASCE*, **114**(8), 1804–1825.

[6] Lie T.T. 1994. Fire resistance of circular steel columns filled with bar-reinforced concrete, *J. Struct. Eng., ASCE*, **120**(5), 1489–1509.

[7] Lie T.T., Irwin R.J. 1995. Fire resistance of rectangular steel columns filled with bar reinforced concrete, *J. Struct. Eng., ASCE*, **121**(5), 797–805.

[8] Yang Y.-F., Han L.-H. 2011. Behaviour of concrete filled steel tubular (CFST) stub columns under eccentric partial compression, *Thin-Walled Struct*, **49**, 379–395.

[9] Han L.-H. 2002. Tests on stub columns of concrete-filled RHS sections, *J. Const. Struct. Res.*, 58, 353–372, 2002.

[10] Han L.-H, Yao G.H., Zhao X. 2005. Tests and calculations for hollow structural steel (HSS) stub columns filled with self-consolidating concrete (SCC), *J. Const. Struct. Res.*, **61**(9), 1241–1269.

[11] Tao Z., Han L.-H., Wang Z.-B. 2005. Experimental behavior of stiffened concrete-filled thin-walled hollow steel structural (HSS) stub columns, *J. Const. Struct. Res.*, **61**, 962–983.

[12] Young, B., Ellobody, E. 2006. Experimental investigation of concrete-filled cold-formed high strength stainless steel tube columns. *J. Const. Steel Res.*, **62**, 484–492.

[13] Lam, D., Gardner, L. 2008. Structural design of stainless steel concrete filled columns. *J. Const. Steel Res.*, **64**, 1275–1282.

[14] Uy, B., Tao, Z., Han, L.-H. 2011. Behaviour of short and slender concrete-filled stainless steel tubular columns. *J. Const. Steel Res.*, **67**, 360–378.

[15] Mursi M., Uy B. 2004. Strength of slender concrete filled high strength steel box columns, *J. Const. Struct. Res.*, **60**, 1825–1848.

[16] Zeghiche J., Chaoui K. 2005. An experimental behaviour of concrete-filled steel tubular columns, *J. Const. Struct. Res.*, **61**(1), 53–66.

[17] Portoles J.M., Romero M.L., Bonet, J.L., Filippou, F.C., Experimental study of high strength concrete-filled circular tubular columns under eccentric loading, *J. Const. Struct. Res.*, **67**, 623–633.

[18] Han L.-H., Li W., Bjorhovde, R. 2014. Developments and advanced applications of concrete-filled steel tubular (CFST) structures: Members, *J. Const. Struct. Res.*, **100**, 211–228.

[19] Comité Européen de Normalisation. 2006. *EN 10210-1:2006 Hot finished structural hollow sections of non-alloy and fine grain steels – Part 1: Technical delivery conditions*. British Standards Institution.

[20] Ruiz-Teran, A. M., Gardner, L. 2008. Elastic buckling of elliptical tubes. *Thin-Walled Struct.*, **46**, 1304–1318.

[21] Chan, T. M., Gardner, L. 2008. Compressive resistance of hot-rolled elliptical hollow sections. *Eng. Struct.*, **30**, 522–532.

[22] Law, K.H., Gardner, L. 2013. Buckling of elliptical hollow section members under combined compression and uniaxial bending. *J. Const. Steel Res.*, **86**, 1–16.

[23] Chan, T. M., Gardner, L. 2009. Bending strength of hot-rolled elliptical hollow sections. *J. Const. Steel Res.*, **64**, 971–986.

[24] Chan, T. M., Gardner L. 2009. Flexural buckling of elliptical hollow section columns. *J. Struct. Eng., ASCE*, **135**(5), 546–557.

[25] Law, K. H., Gardner, L. 2012. Lateral instability of elliptical hollow section beams. *Eng. Struct,*, **37**, 152–166.

[26] Silvestre, N., Gardner, L. 2011. Elastic post-buckling of elliptical tubes. *J. Const. Steel Res.*, **67**, 281–292.

[27] McCann, F., Fang, C., Gardner, L., Silvestre, N. 2016. Local buckling and ultimate strength of slender elliptical hollow sections in compression, *Eng. Struct.*, **111**, 104–118.

[28] Chan T.M., Gardner L., Law K.H. 2010. Structural design of elliptical hollow sections: a review. *Proc. Inst. Civil Engrs Struct. Build.*, **163**(6), 391–402

[29] Gardner, L., Chan, T. M., Wadee, M.A. 2008. Shear response of elliptical hollow sections. *Proc. Inst. Civil Engrs Struct. Build.* **161**(6), 301–309.

[30] Zhao, X.-L., Packer, J. A. 2009. Tests and design of concrete-filled elliptical hollow section stub columns. *Thin-Walled Struct.*, **47**, 617–628.

[31] Uenaka, K. 2014. Experimental study on concrete filled elliptical/oval steel tubular stub columns under compression. *Thin-Walled Struct.*, **78,** 131–137.

[32] Uenaka, K., Tsunokake, H. 2016. Concrete filled elliptical steel tubular members with large diameter-to-thickness ratio subjected to bending. *Structures*, **5**, 58–66.

[33] Jamaluddin, N., Lam, D., Dai, X. H., Ye. J. 2013. An experimental study on elliptical concrete filled columns under axial compression. *J. Const. Steel Res.*, **87** 6–16.

[34] McCann, F., Gardner, L., Qiu, W. 2015. Experimental study of concrete-filled elliptical hollow section beam-columns. *J. Const. Struct. Res.*, **113**, 185–194.

[35] Espinos, A., Romero, M. L., Portolés, J, M., Hospitaler, A. 2014. Ambient and fire behavior of eccentrically loaded elliptical slender concrete-filled tubular columns. *J. Const. Steel Res.*, **100**, 97–107.

[36] Ren, Q.-X., Han, L.-H., Lam, D., Li, W. 2014. Tests on elliptical concrete filled steel tubular (CFST) beams and columns. *J. Const. Steel Res.*, **99**, 149–160.

[37] Sheehan, T, Dai, X. H., Chan, T. M., Lam, D. 2012. Structural response of concrete-filled elliptical steel hollow sections under eccentric compression. *Eng. Struct.* **45**, 314–323.

[38] Hong S., Varma A. 2009. Analytical modeling of the standard fire behavior of loaded CFT columns. *J. Const. Struct. Res.*, **65**, 54–69.

[39] Tao Z., Wang Z., Yu Q. 2013. Finite element modelling of concrete-filled steel stub columns under axial compression, *J. Const. Struct. Res.*, **89**, 121–131.

[40] Dai X., Lam D. 2010. Numerical modelling of the axial compressive behaviour of short concrete-filled elliptical steel columns, *J. Const. Struct. Res.*, **66** (7), 931–942.

[41] Dai X., Lam D., Jamaluddin N., Ye, J. 2014. Numerical analysis of slender elliptical concrete filled columns under axial compression, *Thin-Walled Struct.*, **77**, 26–35.

[42] Espinos A, Romero M.L., Hospitaler A. 2010. Advanced model for predicting the fire response of concrete filled tubular columns, *J. Const. Struct. Res.*, **66**, 1030-1046.

[43] Simulia Inc. 2012. *ABAQUS 6.13 User's Manual*, Simulia.

[44] Han L.H., Yao G.H., Tao Z. 2007. Performance of concrete-filled thin-walled steel tubes under pure torsion", *Thin-Walled Struct*, **45**(1), 24–36.

[45] American Concrete Institute. 2011. *Building Code Requirements for Structural Concrete (ACI 318-11) and Commentary*, Michigan, USA, Farmington Hills.

[46] Bazant Z., Becq-Giraudon E. 2002. Statistical prediction of fracture parameters of concrete and implications for choice of testing standard, *Cement & Conc. Res.*, **32**(4), 529–556.

[47] Comité Européen de Normalisation. 2004. *EN 1992-1-1:2004 Eurocode 2: Design of concrete structures – Part 1-1: General rules and rules for buildings*. British Standards Institution.

[48] Comité Européen de Normalisation. 2005. *EN 1993-1-1:2005 Eurocode 3: Design of steel structures – Part 1-1: General rules and rules for buildings*. British Standards Institution.

[49] Comité Européen de Normalisation. 2008. *EN 1990:2002 Eurocode 0: Basis of structural design*. British Standards Institution.

[50] Afshan, S., Francis, P., Baddoo, N. R. and Gardner, L. 2015. Reliability analysis of structural stainless steel design provisions. *Journal of Constructional Steel Research.*, **114**, 293-304.

[51] Byfield M., Nethercot D. 1997. Material and geometric properties of structural steel for use in design, *The Structural Engineer.*, **75**, 363-367.

[52] El-Reedy M. 2013. Reinforced concrete structural reliability, CRC Press, Boca Raton, FL

[53] Lu R., Luo Y., Conte J.P. 1994. Reliability evaluation of reinforced concrete beams, *Structural safety.*, **14**, 277-298

[54] Arya C. 2009. Design of structural elements, Spon Press, London,

Table captions

Table 1: Properties of specimens tested in experimental programmes
Table 2: Comparison of ultimate loads from experiments and numerical analysis
Table 3: Ranges of variation of parameters for parametric study
Table 4: Reliability analysis results calculated according to EN 1990

Table

Click here to download Table: CFEHS numerical design tables after review.docx

Table 1: Properties of specimens tested in experimental programmes

Specimen	L (mm)	$\bar{\lambda}$	$2a \times 2b \times t$ (mm)	D^*/t	e_y (mm)	e_z (mm)	ρ (%)	Buckling axis	f_y (MPa)	f_c (MPa)	f_s (MPa)	$N_{u,exp}$ (kN)
Reference [34]												
E1:L3-MA-0	3154	1.00	150 × 75 × 6.3	47.62	0	0	0	Major	369.1	36.0	-	761.5
E2:L2-MA-0	2154	0.67	150 × 75 × 6.3	47.62	0	0	0	Major	369.1	32.0	-	886.6
E3:L1-MA-0	1154	0.36	150 × 75 × 6.3	47.62	0	0	0	Major	369.1	33.0	-	1059.3
E4:L3-MA-50	3154	1.00	150 × 75 × 6.3	47.62	0	50	0	Major	369.1	36.5	-	348.5
E5:L2-MA-50	2154	0.68	150 × 75 × 6.3	47.62	0	50	0	Major	369.1	38.3	-	359.8
E6:L1-MA-50	1154	0.36	150 × 75 × 6.3	47.62	0	50	0	Major	369.1	28.7	-	508.6
E7:L3-MA-150	3154	1.00	150 × 75 × 6.3	47.62	0	150	0	Major	369.1	42.7	-	176.3
E8:L2-MA-150	2154	0.67	150 × 75 × 6.3	47.62	0	150	0	Major	369.1	33.2	-	199.2
E9:L1-MA-150	1154	0.36	150 × 75 × 6.3	47.62	0	150	0	Major	369.1	36.2	-	222.7
E10:L3-MI-0	3154	1.78	150 × 75 × 6.3	47.62	0	0	0	Minor	369.1	40.6	-	349.0
E11:L2-MI-0	2154	1.20	150 × 75 × 6.3	47.62	0	0	0	Minor	369.1	35.4	-	664.3
E12:L1-MI-0	1154	0.65	150 × 75 × 6.3	47.62	0	0	0	Minor	369.1	36.0	-	831.3
E13:L3-MI-25	3154	1.79	150 × 75 × 6.3	47.62	25	0	0	Minor	369.1	41.8	-	222.5
E14:L2-MI-25	2154	1.20	150 × 75 × 6.3	47.62	25	0	0	Minor	369.1	37.0	-	337.9
E15:L1-MI-25	1154	0.63	150 × 75 × 6.3	47.62	25	0	0	Minor	369.1	32.2	-	460.3
E16:L3-MI-50	3154	1.73	150 × 75 × 6.3	47.62	50	0	0	Minor	369.1	33.0	-	167.9
E17:L2-MI-50	2154	1.19	150 × 75 × 6.3	47.62	50	0	0	Minor	369.1	33.1	-	245.8
E18:L1-MI-50	1154	0.63	150 × 75 × 6.3	47.62	50	0	0	Minor	369.1	28.7	-	321.6
E19:L3-MA-50-R	3154	0.93	150 × 75 × 6.3	47.62	0	50	4.7	Major	369.1	32.6	561.7	370.2
E20:L2-MA-50-R	2154	0.65	150 × 75 × 6.3	47.62	0	50	4.7	Major	369.1	38.7	561.7	482.3
E21:L1-MA-50-R	1154	0.35	150 × 75 × 6.3	47.62	0	50	4.7	Major	369.1	35.9	561.7	578.6
E22:L3-MI-25-R	3154	1.72	150 × 75 × 6.3	47.62	25	0	4.7	Minor	369.1	31.8	561.7	225.7
E23:L2-MI-25-R	2154	1.19	150 × 75 × 6.3	47.62	25	0	4.7	Minor	369.1	35.8	561.7	353.3
E24:L1-MI-25-R	1154	0.64	150 × 75 × 6.3	47.62	25	0	4.7	Minor	369.1	36.1	561.7	492.7
Reference [35]												
E-50	2135	0.81	220 × 110 × 12	36.67	50	0	0	Minor	372.5	37.6	-	810
E-20	2135	0.79	220 × 110 × 12	36.67	20	0	0	Minor	347.5	38.2	-	1168
E-00	2135	0.79	220 × 110 × 12	36.67	0	0	0	Minor	348.1	37.1	-	2331
RE-50	2135	0.83	220 × 110 × 12	36.67	50	0	2.4	Minor	369.7	39.4	519	777
RE-20	2135	0.83	220 × 110 × 12	36.67	20	0	2.4	Minor	369.7	39.2	519	1174
RE-00	2135	0.84	220 × 110 × 12	36.67	0	0	2.4	Minor	372.5	39.5	519	2071
Reference [36]												

ec1-1	3600	1.00	192 × 124 × 3.82	77.82	0	0	0	Major	439.3	50.0	-	1121
ec1-2	3600	1.00	192 × 124 × 3.82	77.82	0	0	0	Major	439.3	50.0	-	1157
ec2-1	2700	0.68	192 × 124 × 3.82	77.82	0	0	0	Major	439.3	50.0	-	1389
ec2-2	2700	0.68	192 × 124 × 3.82	77.82	0	0	0	Major	439.3	50.0	-	1322
ec3-1	1800	0.50	192 × 124 × 3.82	77.82	0	0	0	Major	439.3	50.0	-	1896
ec3-2	1800	0.50	192 × 124 × 3.82	77.82	0	0	0	Major	439.3	50.0	-	1829
ec4-1	3600	1.00	192 × 124 × 3.82	77.82	0	48	0	Major	439.3	50.0	-	632
ec4-2	3600	1.00	192 × 124 × 3.82	77.82	0	48	0	Major	439.3	50.0	-	641
ec5-1	3600	1.00	192 × 124 × 3.82	77.82	0	144	0	Major	439.3	50.0	-	325
ec5-2	3600	1.00	192 × 124 × 3.82	77.82	0	144	0	Major	439.3	50.0	-	343
ec6-1	2700	0.68	192 × 124 × 3.82	77.82	0	48	0	Major	439.3	50.0	-	776
ec6-2	2700	0.68	192 × 124 × 3.82	77.82	0	48	0	Major	439.3	50.0	-	788
ec7-1	1800	0.50	192 × 124 × 3.82	77.82	0	48	0	Major	439.3	50.0	-	972
ec7-2	1800	0.50	192 × 124 × 3.82	77.82	0	48	0	Major	439.3	50.0	-	961

* Equivalent diameter $D=2a^2/b$ is adopted

Table 2: Comparison of ultimate loads from experiments and numerical analysis

Specimen	$N_{u,exp}$ (kN)	$N_{u,FEA}$ (kN)	$N_{u,exp}$ / $N_{u,FEA}$
Reference [34]			
E1:L3-MA-0	762	704	1.08
E2:L2-MA-0	887	914	0.97
E3:L1-MA-0	1059	1020	1.04
E4:L3-MA-50	349	306	1.14
E5:L2-MA-50	360	384	0.94
E6:L1-MA-50	509	452	1.13
E7:L3-MA-150	176	159	1.11
E8:L2-MA-150	199	179	1.11
E9:L1-MA-150	223	208	1.07
E10:L3-MI-0	349	330	1.06
E11:L2-MI-0	664	588	1.13
E12:L1-MI-0	831	873	0.95
E13:L3-MI-25	223	193	1.15
E14:L2-MI-25	338	280	1.21
E15:L1-MI-25	460	393	1.17
E16:L3-MI-50	168	147	1.14
E17:L2-MI-50	246	201	1.22
E18:L1-MI-50	322	268	1.20
E19:L3-MA-50-R	370	341	1.09
E20:L2-MA-50-R	482	439	1.10
E21:L1-MA-50-R	579	535	1.08
E22:L3-MI-25-R	226	189	1.19
E23:L2-MI-25-R	353	301	1.18
E24:L1-MI-25-R	493	446	1.10
Reference [35]			
E-00	2331	2078	1.12
E-20	1168	1157	1.01
E-50	810	819	0.99
RE-00	2071	2024	1.02
RE-20	1174	1244	0.94
RE-50	777	842	0.92
Reference [36]			
ec1-1	1121	1135	1.00
ec1-2	1157	1135	1.03
ec2-1	1389	1366	1.03
ec2-2	1322	1366	0.98
ec3-1	1896	1531	1.26
ec3-2	1829	1531	1.21
ec4-1	632	546	1.17
ec4-2	641	546	1.19
ec5-1	325	278	1.18
ec5-2	343	278	1.24

ec6-1	776	663	1.18
ec6-2	788	663	1.20
ec7-1	972	796	1.22
ec7-2	961	796	1.20
Average			1.11
Standard deviation			0.09

Table 3: Ranges of variation of parameters for parametric study

$2a \times 2b$ (mm)	220 × 110	480 × 240
t (mm)	6.3; 12.5*	12.5; 14.2
$\bar{\lambda}_y$	0.2; 0.5; 0.8; 1; 1.2	0.2; 0.5; 0.8; 1.1
u_s (mm)	30	55; 65
ρ (%)	0; 2.5; 5	
$e/2a$; $e/2b$	0; 0.25; 0.50	
Buckling axis	major; minor	
f_y (MPa)	355	
f_c (MPa)	30	
f_s (MPa)	500	
B.C.	pinned-pinned	

*220 × 110 × 12.5 specimens were not modelled with reinforcement since EN 1992-1-1 requirements regarding minimum bar spacings cannot be met

Table 4: Reliability analysis results calculated according to EN 1990

Loading condition	Sample type	Sample number	$k_{d,n}$	b	V_δ	γ_{M1}
(a) Axial compression	Test	13	4.078	1.166	0.044	1.014
	Test and FEA	133	3.165	1.029	0.048	1.016
(b) Combined compression	Test	30	3.452	1.086	0.053	1.050
and uniaxial bending	Test and FEA	186	3.143	1.048	0.054	0.993

Figure captions

Click here to download Figure: CFEHS numerical design figure captions after review.docx

Figure 1: Cross-sectional geometry of CFEHS tests specimens with reinforcement and eccentric load positions.

Figure 2: Typical measured stress-strain curve of steel and the multi-linear model adopted in FE analysis.

Figure 3: Typical stress-strain curves of unconfined and confined (by an EHS) concrete

Figure 4: Model in ABAQUS [43] of a column intended to buckle about its major axis.

Figure 5: Comparison of ultimate loads from experiments and numerical analysis

Figure 6: Comparison between test and FE load-lateral deflection responses for specimens [34] buckling about the major axis

Figure 7: Comparison between test and FE load-lateral deflection responses for specimens [34] buckling about the minor axis

Figure 8: Comparison of graphs of load against axial displacement for specimens [34] containing steel reinforcement

Figure 9: Comparison of deformed beam-columns (left) as observed in experiments and (right) predicted by numerical model for specimen E6:L1-MA-50 [34]

Figure 10: Cross-sectional geometry and positions of reinforcing bars and eccentric loads for parametric study specimens

Figure 11: Comparison of normalised ultimate loads Nu from experiments and numerical parametric study with EN 1993-1-1 [48] buckling curves

Figure 12: Comparison of experimental and numerical ultimate loads with design ultimate loads for members under axial compression determined using EN 1993-1-1 [48] curves b and c

Figure 13: Variation with slenderness of ratio of ultimate loads Nu from experiments and numerical analysis to design resistances Nu,EC4 for members under axial compression determined using EN 1993-1-1 [48] curves b and c

Figure 14: Comparison of experimental and numerical ultimate loads with design ultimate loads for members under combined compression and uniaxial bending

Figure 15: Variation of ratio of ultimate loads from experiments and numerical analysis to predictions of EN 1994-1-1 [1] with slenderness for members under combined compression and uniaxial bending

Figure 16: Variation of ratio of numerical parametric study ultimate loads to design ultimate loads with load eccentricity

Figure 17: Variation of ratio of numerical parametric study ultimate loads to design ultimate loads with reinforcement ratio

Figure
Click here to download Figure: CFEHS numerical design figures after review.docx

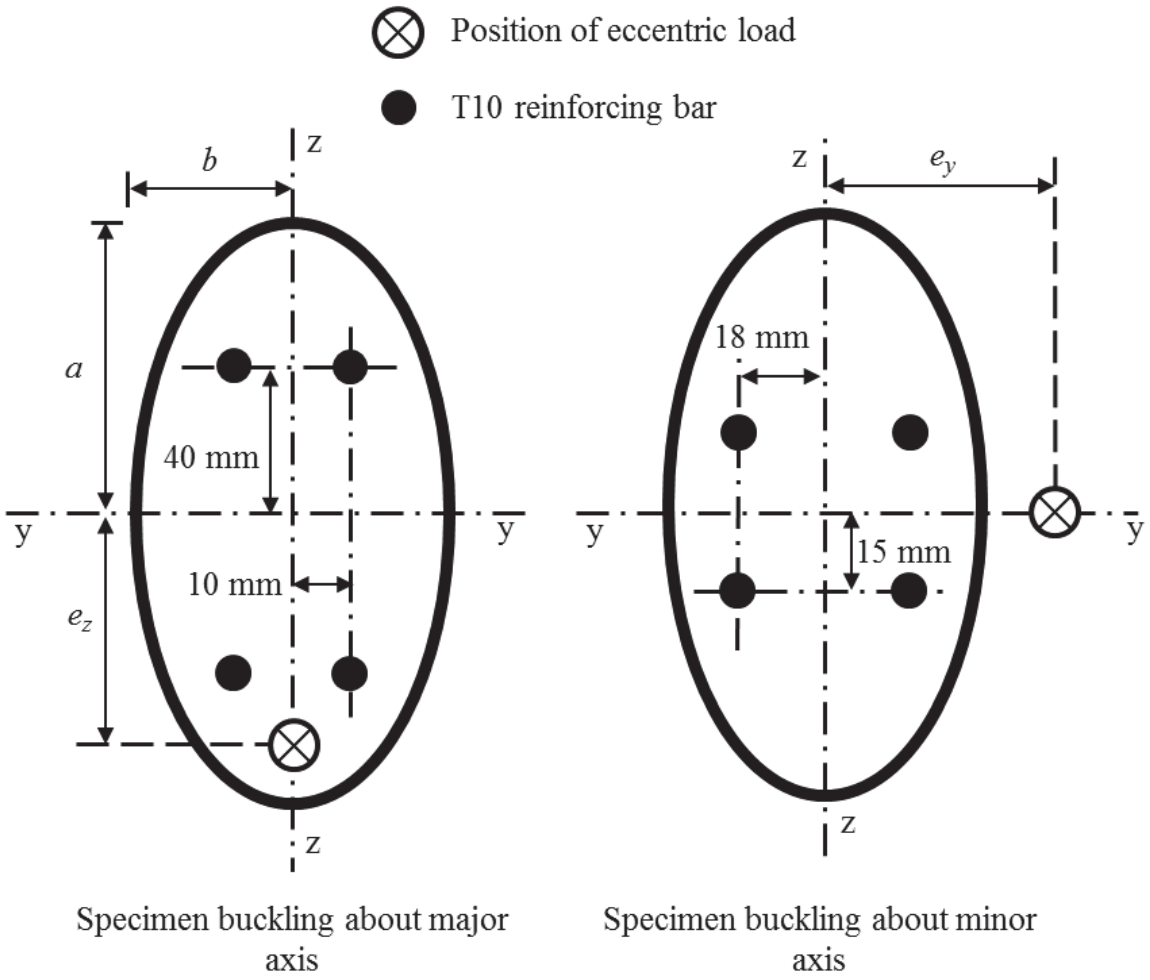

Figure 1: Cross-sectional geometry of CFEHS tests specimens with reinforcement and eccentric load positions

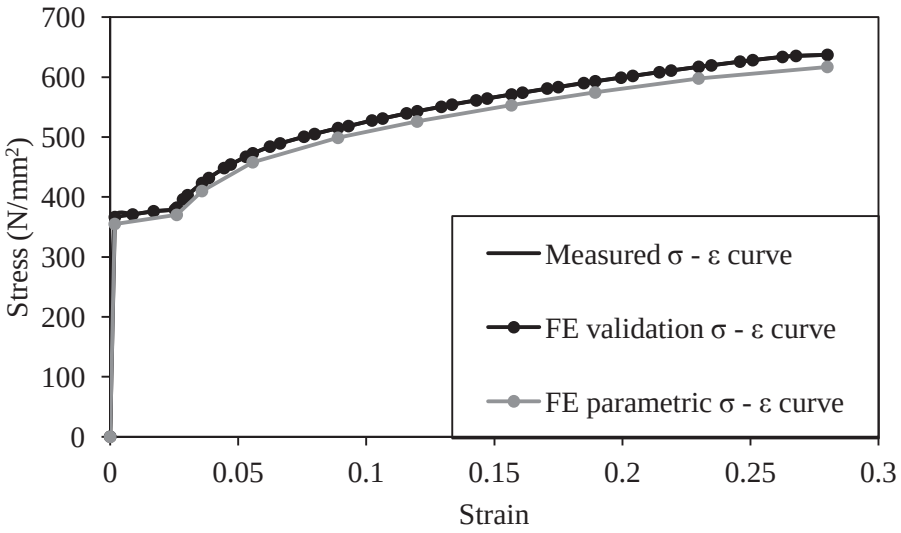

Figure 2: Typical measured stress-strain curve of steel and the multi-linear model adopted in FE analysis

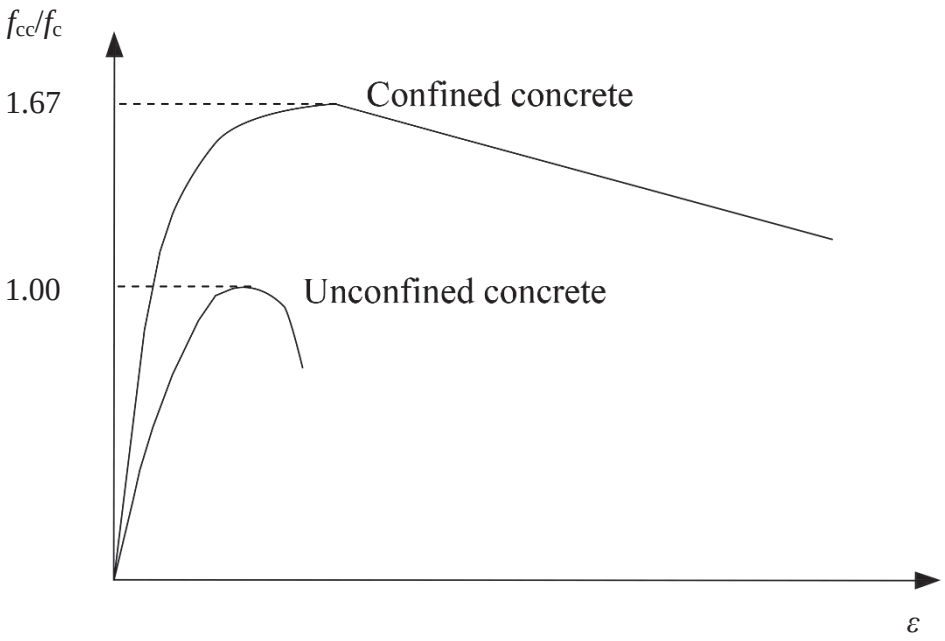

Figure 3: Typical stress-strain curves of unconfined and confined (by an EHS) concrete

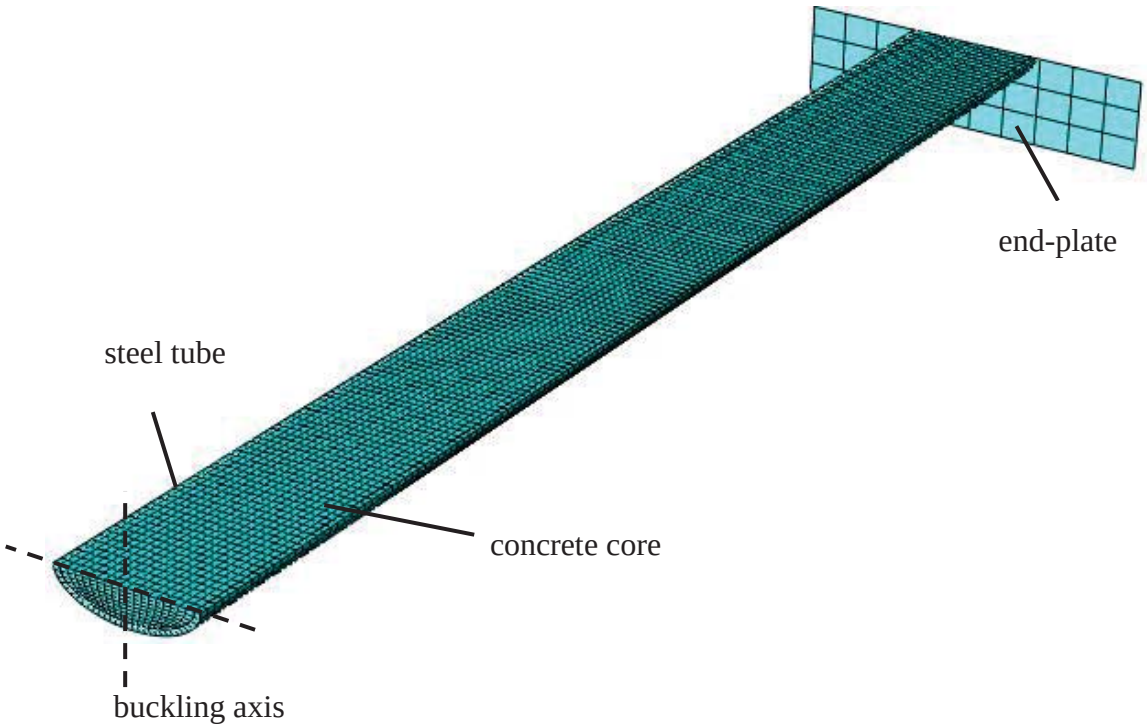

Figure 4: Model in ABAQUS [43] of a column intended to buckle about its major axis

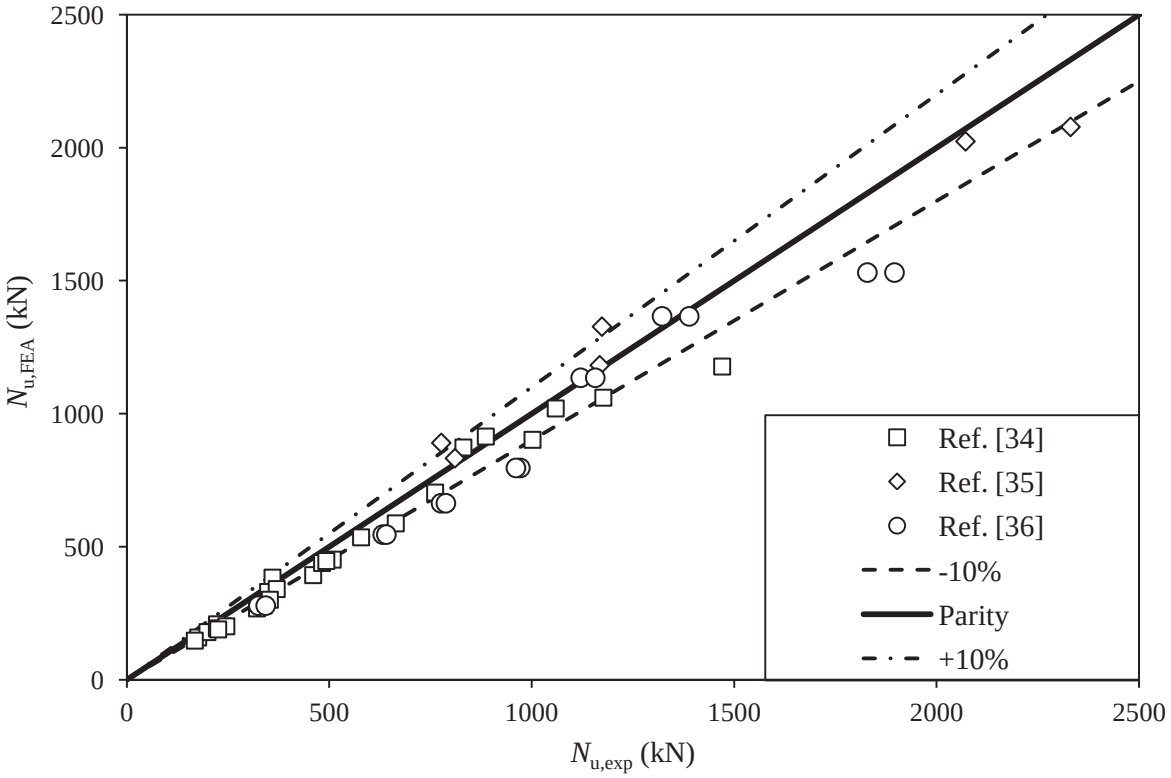

Figure 5: Comparison of ultimate loads from experiments and numerical analysis

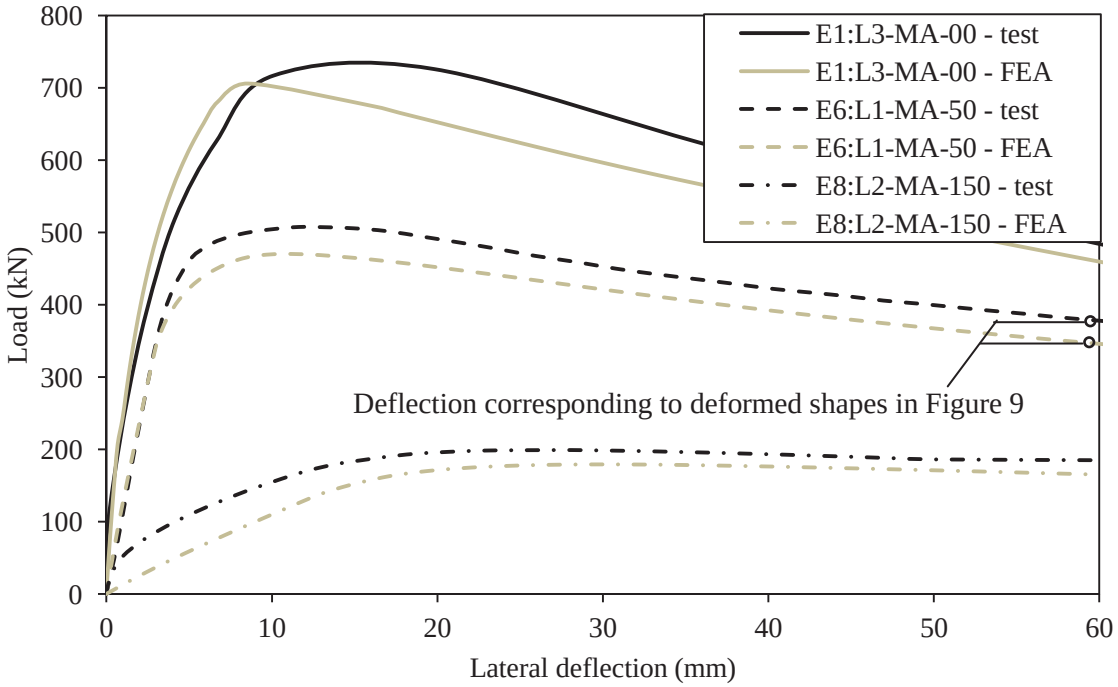

Figure 6: Comparison between test and FE load-lateral deflection responses for specimens [34] buckling about the major axis

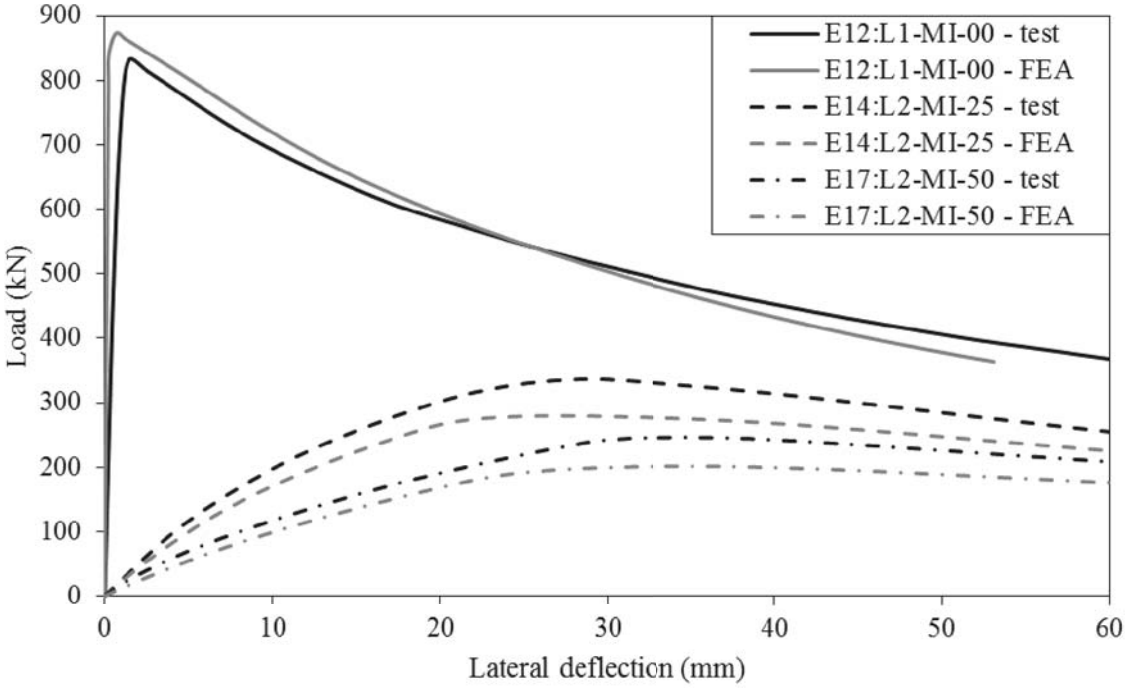

Figure 7: Comparison between test and FE load-lateral deflection responses for specimens [34] buckling about the minor axis

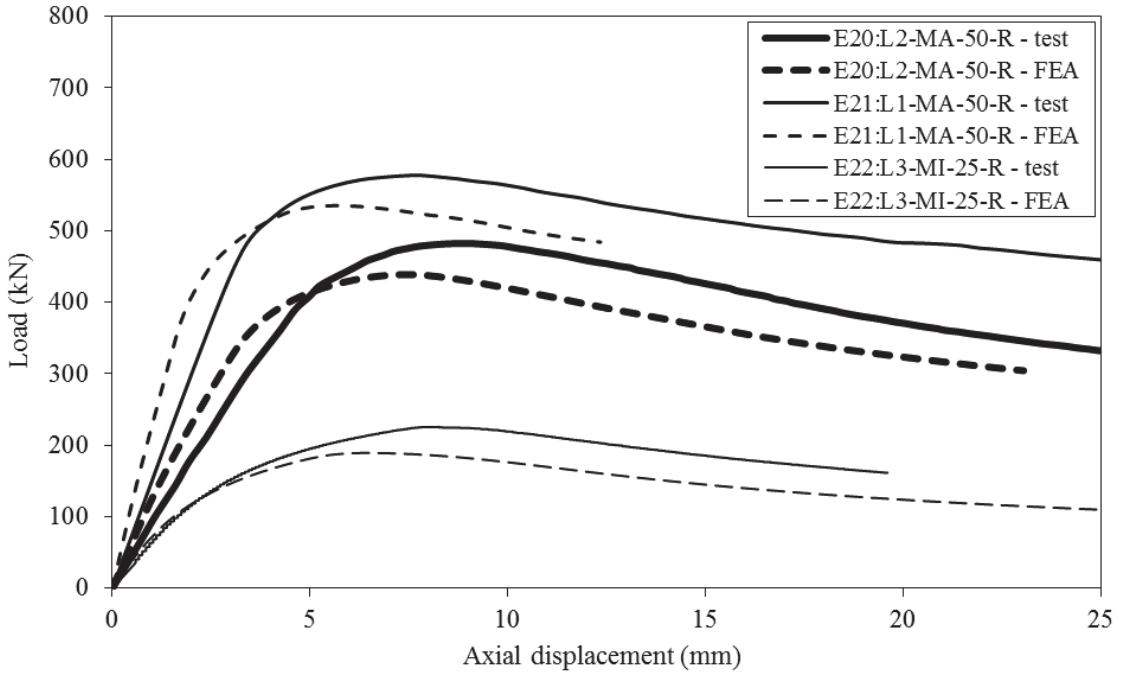

Figure 8: Comparison of graphs of load against axial displacement for specimens [34] containing steel reinforcement

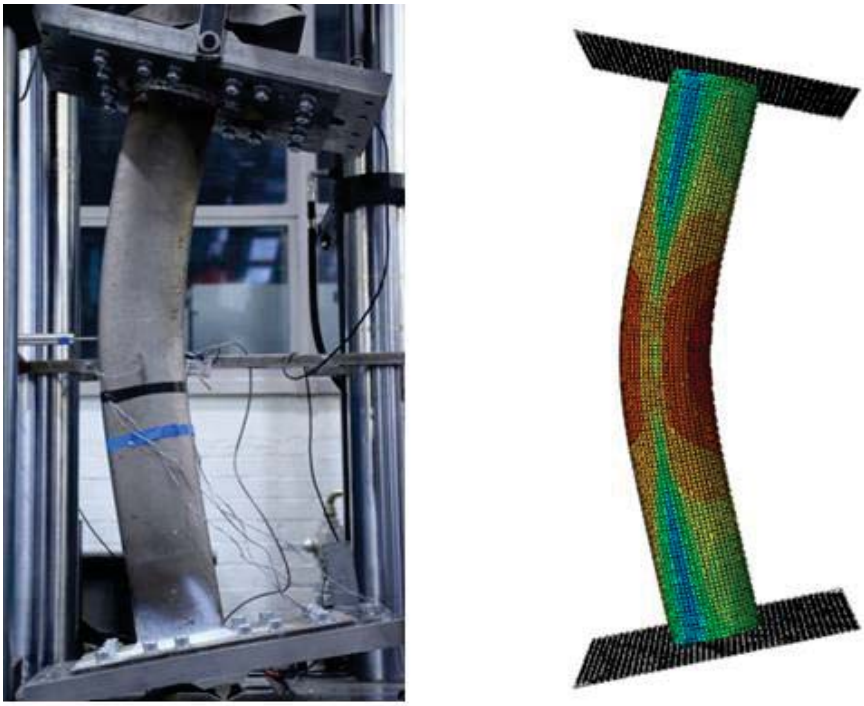

Figure 9: Comparison of deformed beam-columns (left) as observed in experiments and (right) predicted by numerical model for specimen E6:L1-MA-50 [34]

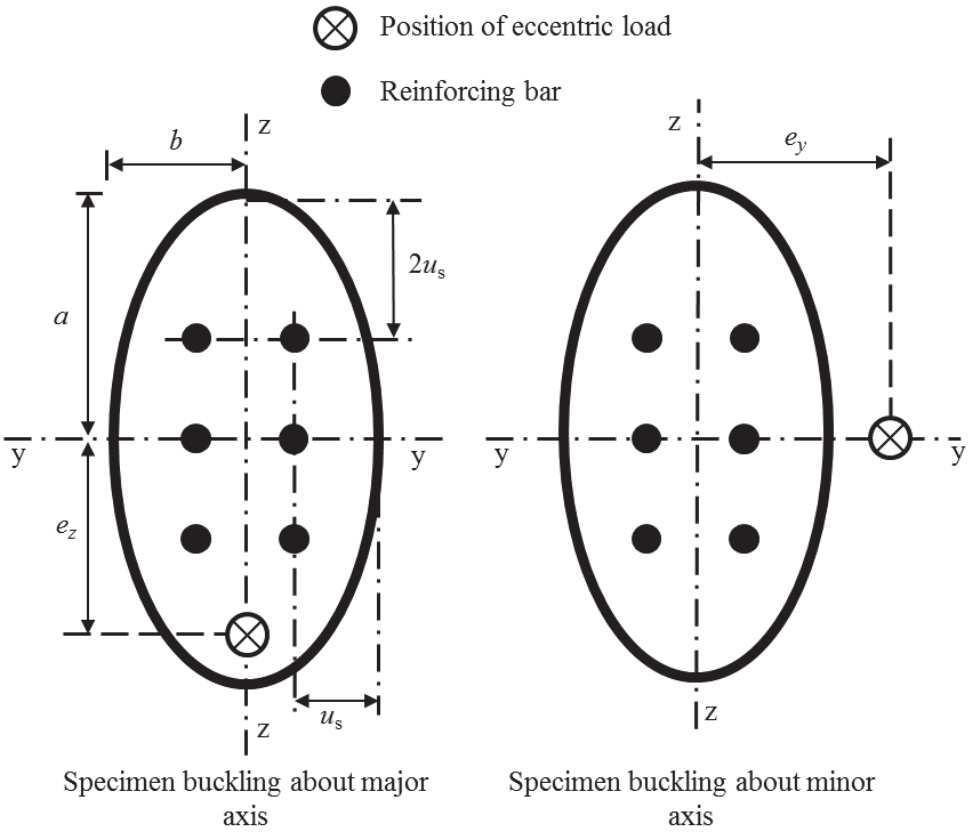

Figure 10: Cross-sectional geometry and positions of reinforcing bars and eccentric loads for parametric study specimens

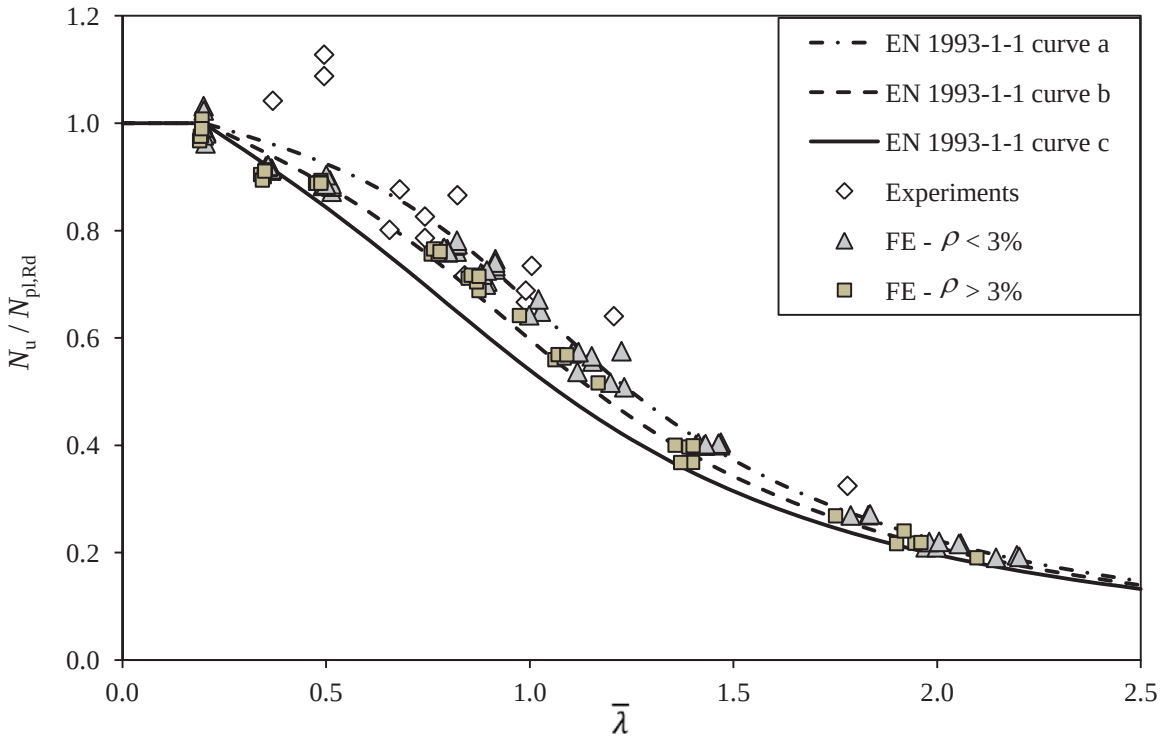

Figure 11: Comparison of normalised ultimate loads N_u from experiments and numerical parametric study with EN 1993-1-1 [48] buckling curves

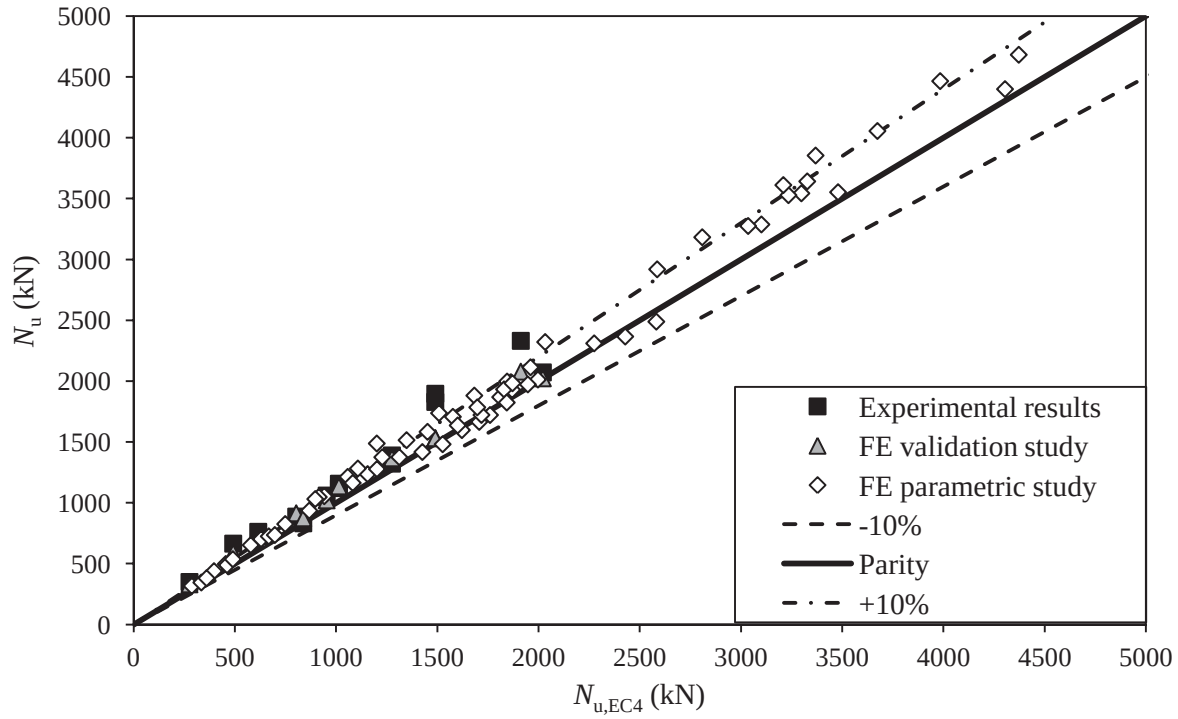

Figure 12: Comparison of experimental and numerical ultimate loads with design ultimate loads for members under axial compression determined using EN 1993-1-1 [48] curves b and c

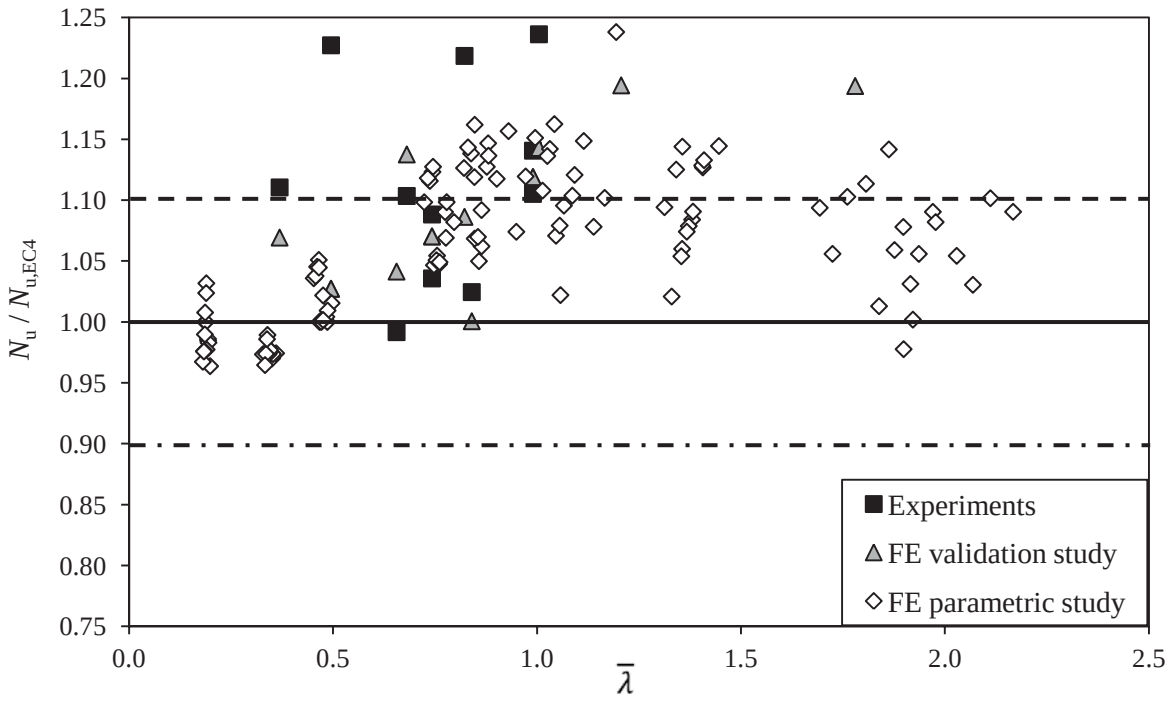

Figure 13: Variation with slenderness of ratio of ultimate loads N_u from experiments and numerical analysis to design resistances $N_{u,EC4}$ for members under axial compression determined using EN 1993-1-1 [48] curves b and c

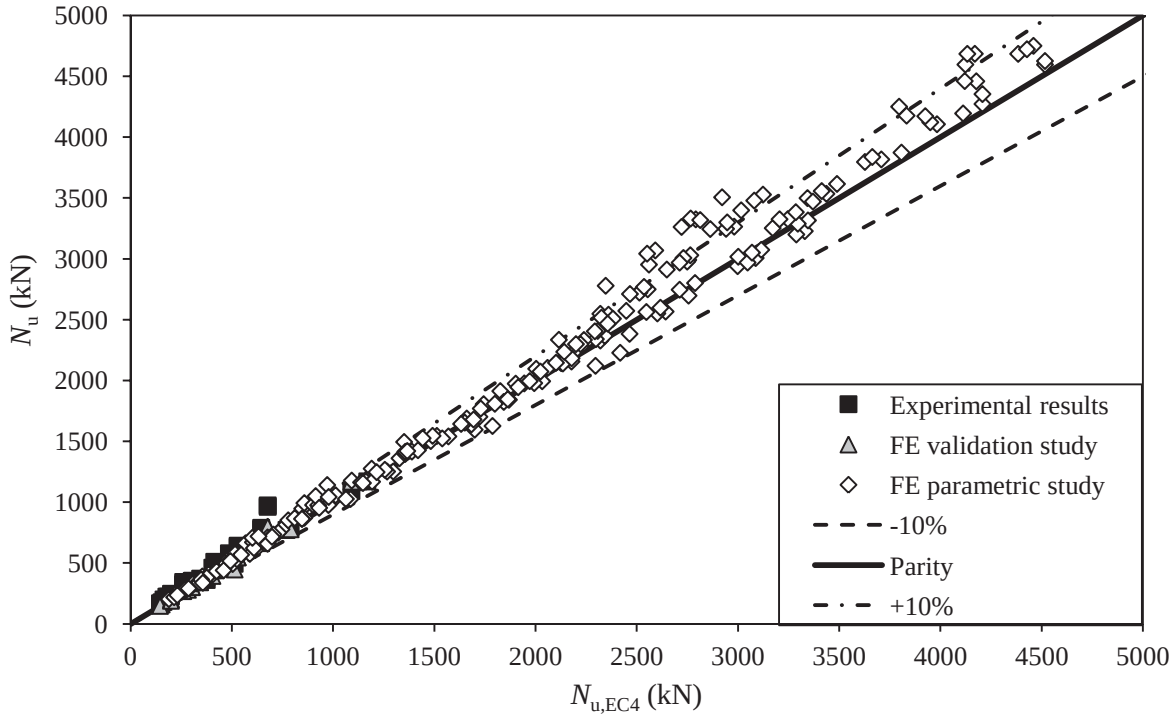

Figure 14: Comparison of experimental and numerical ultimate loads with design ultimate loads for members under combined compression and uniaxial bending

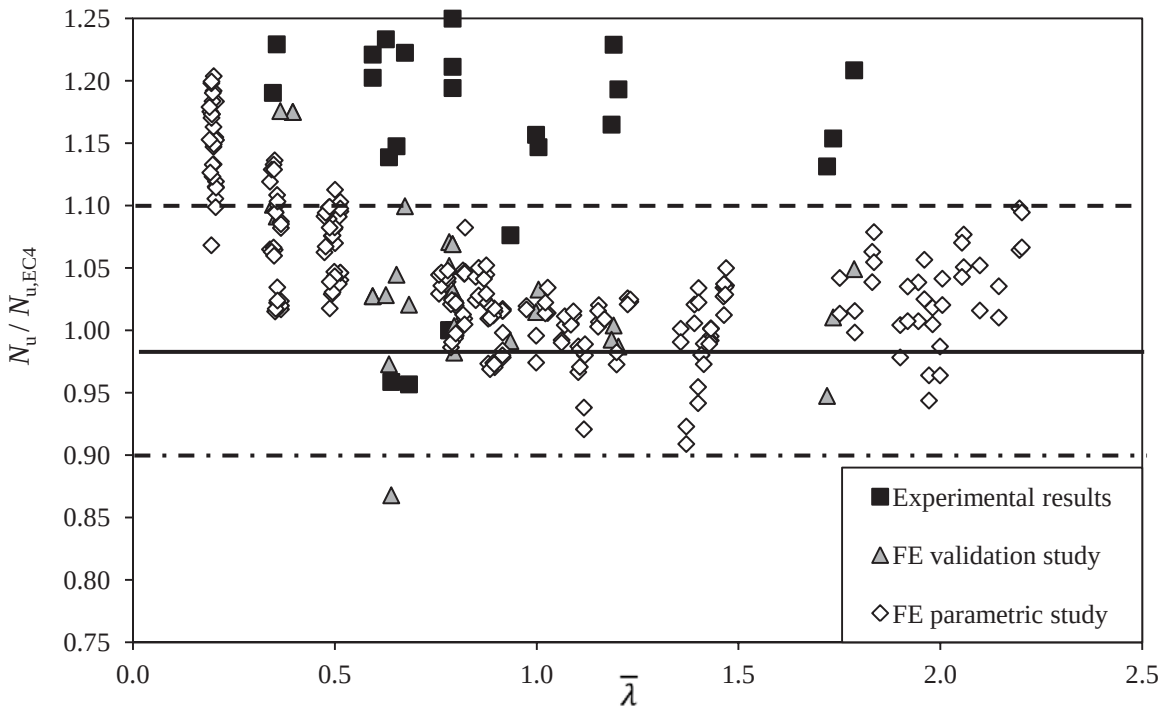

Figure 15: Variation of ratio of ultimate loads from experiments and numerical analysis to predictions of EN 1994-1-1 [1] with slenderness for members under combined compression and uniaxial bending

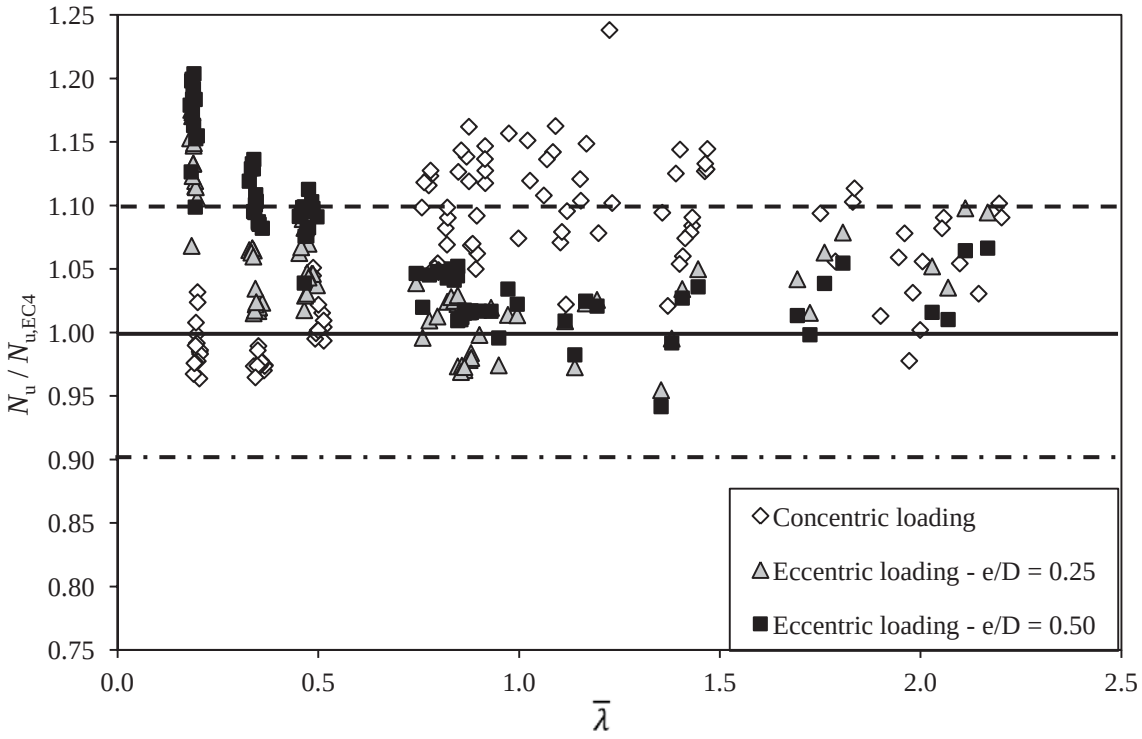

Figure 16: Variation of ratio of numerical parametric study ultimate loads to design ultimate loads with load eccentricity

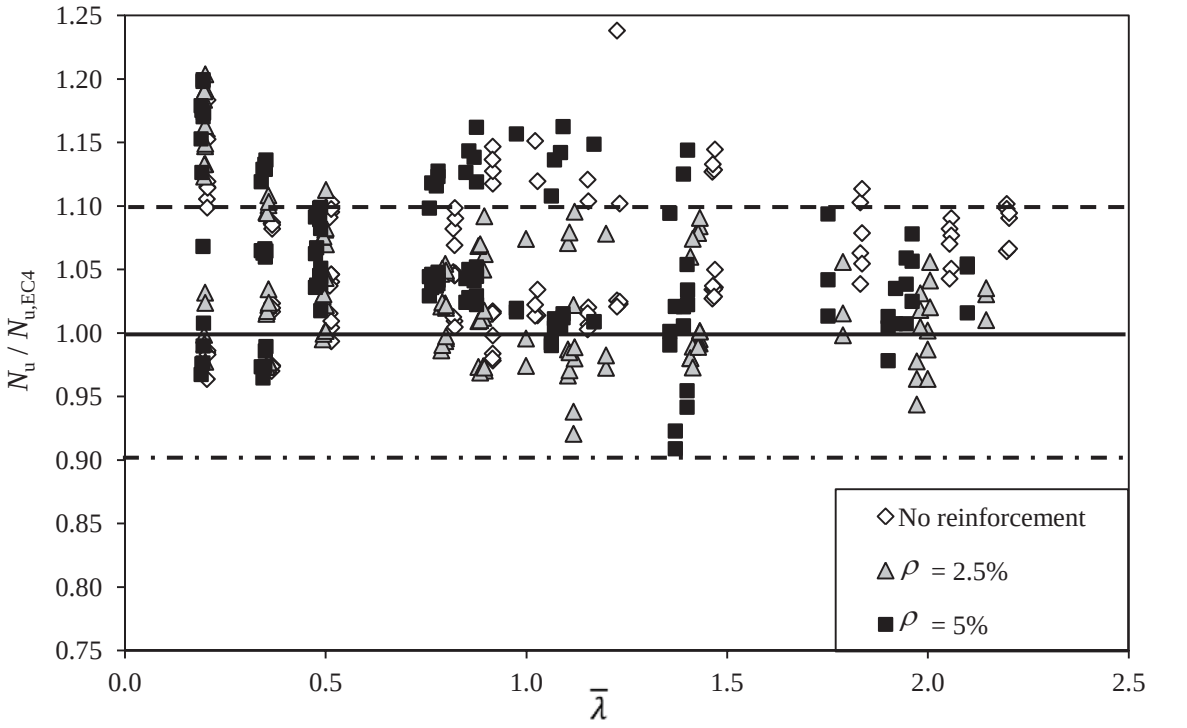

Figure 17: Variation of ratio of numerical parametric study ultimate loads to design ultimate loads with reinforcement ratio